



Three-dimensional P- and S-wave velocity structures beneath the Ryukyu arc

Masaki Nakamura^{a,*}, Yasuhiro Yoshida^a, Dapeng Zhao^b,
Hiroshi Katao^c, Sou Nishimura^c

^a*Meteorological Research Institute, Nagamine 1-1, Tsukuba 305-0052, Japan*

^b*Geodynamics Research Center, Ehime University, Matsuyama 790-8577, Japan*

^c*Kyoto University, Gokasyo, Uji, Kyoto 611-0011, Japan*

Received 12 July 2002; accepted 11 April 2003

Abstract

The three-dimensional (3-D) P- and S-wave velocity structures beneath the Ryukyu arc are determined by seismic wave travel time tomography, using recordings on temporary stations in the sea area as well as those on routine stations. For the inversion, we explicitly define the upper boundary of the Philippine Sea slab. As a result, we obtain 3-D P- and S-wave velocity structures beneath the Ryukyu arc, which are more accurate than previous ones. P- and S-wave low velocity zones and high V_p/V_s zones exist just beneath active volcanoes at about 10 km depth, which show the influence of arc magmas beneath the volcanoes. Prominent P- and S-wave low velocity zones exist along the Okinawa trough at about 50 km depth, where V_p/V_s values are high. The low-velocity and high V_p/V_s anomalies will represent some mantle materials flow upward from the depth greater than 50 km along the trough. Low velocity anomalies are visible beneath the Philippine Sea slab, which are possibly associated with small-scale mantle convections.

© 2003 Elsevier B.V. All rights reserved.

Keywords: Ryukyu arc; Seismic wave travel time tomography; Okinawa trough; Philippine Sea slab

1. Introduction

The Ryukyu arc is located southeast of the Eurasian plate, and the Philippine Sea plate is subducting northwestward beneath the Eurasian plate from the Ryukyu trench (Fig. 1). Moreover, the Okinawa trough, which is a backarc basin whose rifting is still in progress, exists northwest of the arc

(e.g. Park et al., 1998). The regional stress field caused by motions of these plates produces intense seismic activity and active crustal movement in the region.

In order to better understand the seismotectonics of a region, it is useful to determine the three-dimensional (3-D) seismic wave velocity structure of the crust and upper mantle. Several researchers have determined 3-D velocity structures beneath a region including the Ryukyu arc by using the travel time tomography method (e.g. Kamiya et al., 1989; Kamiya, 1991; Nakamura et al., 2000). However,

* Corresponding author. Fax: +81-29-851-3730.

E-mail address: mnakamur@mri-jma.go.jp (M. Nakamura).

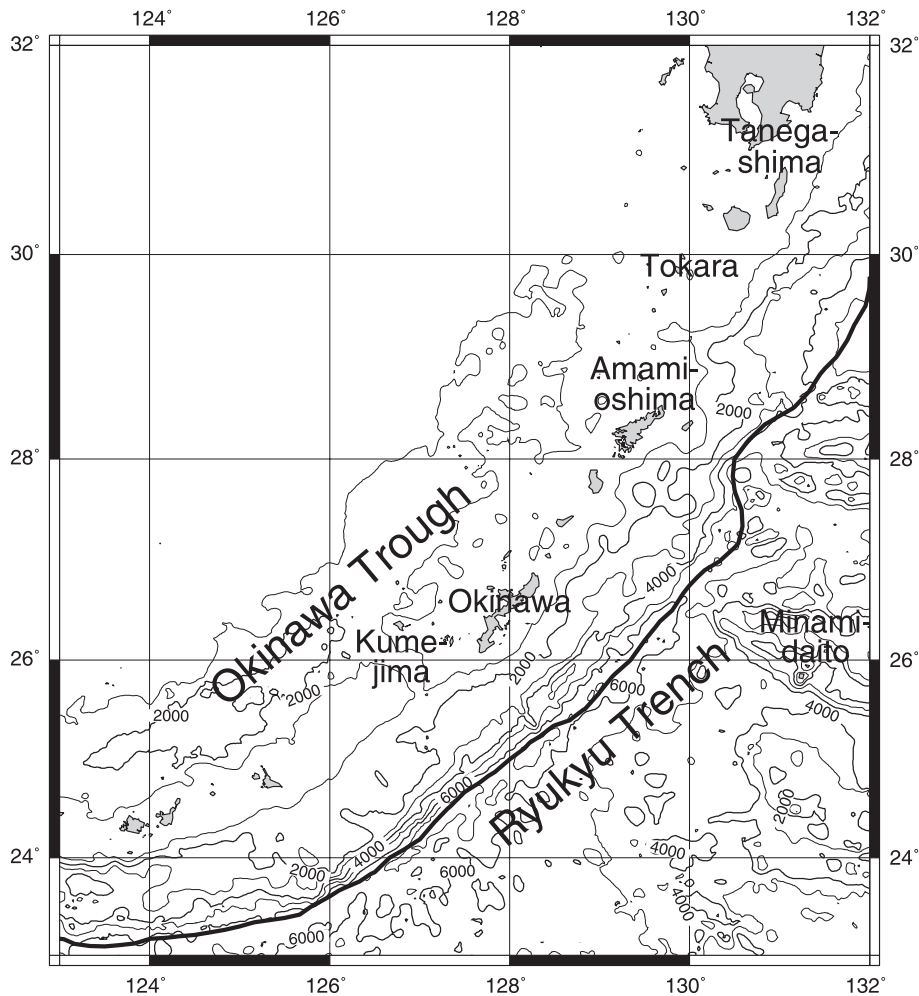


Fig. 1. An index map around the Ryukyu arc. The thick solid line indicates the Ryukyu trench. Bathymetry (Smith and Sandwell, 1994, 1997) is drawn simultaneously (unit: m).

these researchers did not discuss characteristics of the structure of the Ryukyu region, because of the low resolution caused by the poor distribution of seismic stations.

In this study, we revealed 3-D P- and S-wave velocity structures beneath the Ryukyu arc by applying the method of Zhao et al. (1994) with a spatial resolution of about 30 km. We used a large number of data obtained by temporary stations in the sea area as well as those obtained by land stations. Based on the determined velocity structures, we discuss the structure and origin of active volcanoes, Okinawa trough and seismicity.

2. Data and method

We applied the method developed by Zhao et al. (1994) to the area from 23°N to 32°N, from 123°E to 132°E and depth from 0 to 300 km. This method determines P- or S-wave velocity at each point of a 3-D grid and hypocenter parameters by a simultaneous inversion. Moreover, it can deal with a velocity model with multiple velocity discontinuities, for example, the Conrad, the Moho and the subducting slab boundary. A 3-D ray tracing technique is used to compute travel times and ray paths, and the LSQR algorithm (Paige and Saunders, 1982) is

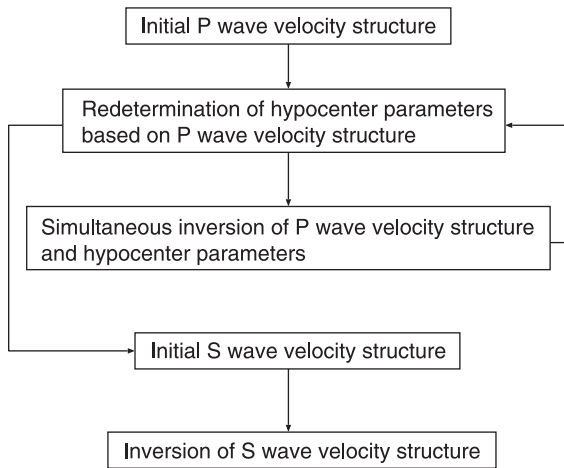


Fig. 2. The outline of the procedure in this study.

adopted to conduct inversions of the observation equation.

In this study we collected hypocenter parameters and high-quality P- and S-wave arrival times. We constructed depth distribution data of the Conrad, the Moho and the upper boundary of the subducting Philippine Sea slab. Using these data, we determined the 3-D P-wave velocity structure and then redetermined the hypocenter parameters. After that, we determined the 3-D S-wave velocity structure. The outline of the procedure is shown in Fig. 2.

We can categorize earthquakes that were used in this study into the following: (1) Earthquakes of which hypocenter parameters were determined by temporary pop-up type ocean bottom seismometer networks. Specifically, they were determined by temporary observation networks near Tanegashima island (from April to June in 1999), southeast off Tokara islands (from August to October in 2000) and southwest off Kumejima island (from May to July in 2001). (2) Earthquakes of which those were determined by depth phases by ISC. (2-1) Some of them that could not be determined stably only by stations in the modeling area. (2-2) The others. (3) Blasts of which those were determined by fixing depths to 0 km. (4) The other regional earthquakes of which those were determined by Japan Meteorological Agency (JMA). (5) Teleseismic events of which those

were determined by ISC and USGS. Note that we used arrival times that JMA manually picked on seismograms recorded by the high sensitivity seismometers.

From earthquakes which belong to the above categories (1), (2) and (3), we chose one earthquake from every block of 0.1° horizontal interval and of 20 km vertical interval, in the area from 23.2°N to 31.8°N , from 123.2°E to 131.8°E and depth from 0 to 260 km, based on the accuracy of hypocenter parameters, and quality and quantity of arrival times. For blocks from which we could not choose earthquakes, we chose earthquakes from JMA earthquake catalogs covering from 1995 to March in 2002, referring to the same judgement (the category (4)). As for (5) teleseismic events, using ISC and USGS catalogs, we selected earthquakes whose magnitudes were relatively large and whose phases could be identified clearly at stations in the study area. Then, we selected the earthquakes with epicentral distances from 30° to 90° to avoid the effects of complex structures of the core–mantle boundary and the upper mantle, as mentioned in Zhao et al. (1994).

Table 1 shows the numbers of events and their arrival times for each of the above category. Fig. 3

Table 1
Numbers of events and arrival times, and constraints for hypocenter determination

Data type ^a	Events	P phases	S phases	Constraint for hypocenter determination
(1) Obs	296	2864	2033	nothing
(2-1) ISC-1	27	285	182	location parameters are fixed; origin time is constrained by damping
(2-2) ISC-2	276	3058	1464	depth is fixed; other parameters are constrained by damping
(3) Blast	15	61	28	depth is fixed to 0 km
(4) Regional	2347	18,284	15,099	nothing
(5) Teleseismic	152	1365	0	all parameters are fixed
Total	3113	25,917	18,806	–

^a Data types are defined in Section 2.

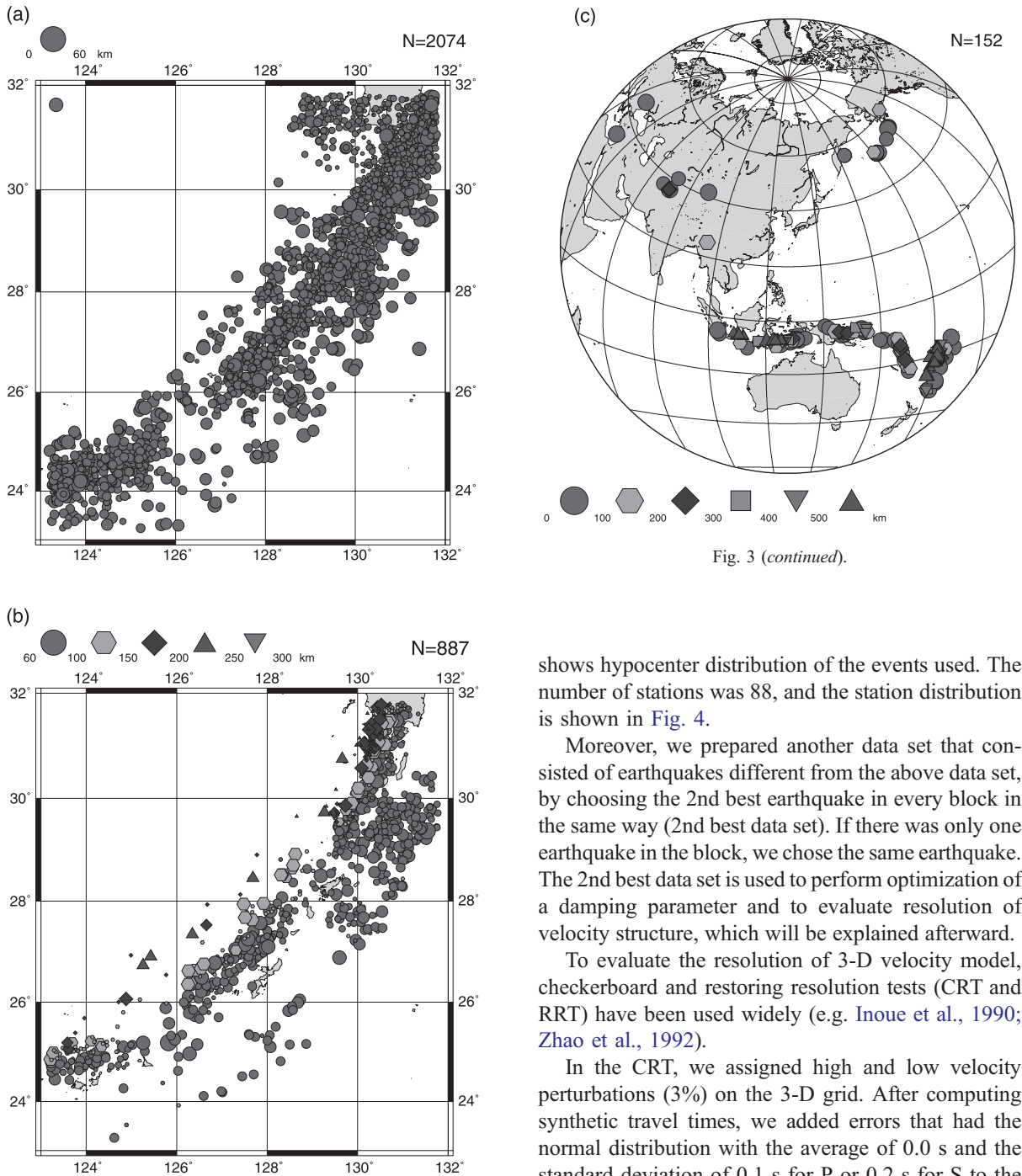


Fig. 3 (continued).

Fig. 3. Epicenter distribution of local and regional earthquakes, (a) which occurred shallower than 60 km and (b) which occurred deeper than 60 km, and (c) that of telesismic events, used in this study.

shows hypocenter distribution of the events used. The number of stations was 88, and the station distribution is shown in Fig. 4.

Moreover, we prepared another data set that consisted of earthquakes different from the above data set, by choosing the 2nd best earthquake in every block in the same way (2nd best data set). If there was only one earthquake in the block, we chose the same earthquake. The 2nd best data set is used to perform optimization of a damping parameter and to evaluate resolution of velocity structure, which will be explained afterward.

To evaluate the resolution of 3-D velocity model, checkerboard and restoring resolution tests (CRT and RRT) have been used widely (e.g. Inoue et al., 1990; Zhao et al., 1992).

In the CRT, we assigned high and low velocity perturbations (3%) on the 3-D grid. After computing synthetic travel times, we added errors that had the normal distribution with the average of 0.0 s and the standard deviation of 0.1 s for P or 0.2 s for S to the theoretical travel times, considering that arrival times had these errors.

A procedure of the RRT was as follows. At first, based on the determined velocity structure, we

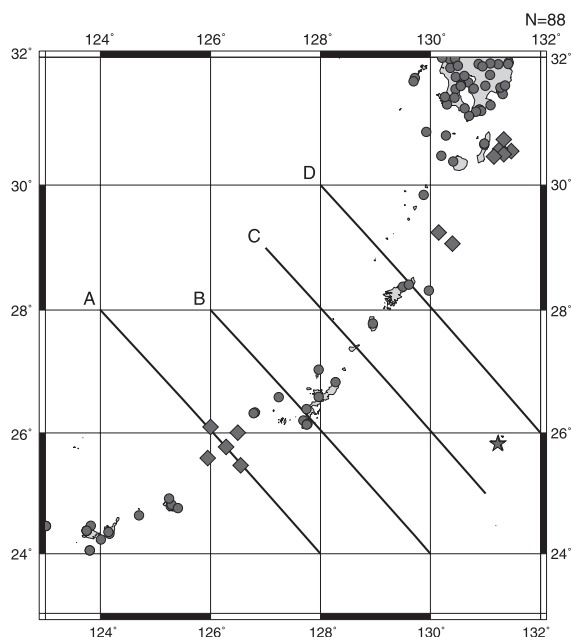


Fig. 4. Station distribution used in this study. Diamonds indicate stations where pop-up type ocean bottom seismometers were temporally installed. Stars indicate stations in Minami-daito island. The locations of the cross sections (the lines A, B, C and D), which are used in the following figures, are also shown.

computed theoretical travel times for hypocenter parameters and arrival times that were used in the analysis. Then, using this data set, we determined velocity structure in the same way, and checked how the original velocity structure was reproduced. We added errors to the original assumed data like the CRT.

In addition to these, we evaluated resolution by analyzing the 2nd best data set by the same way and comparing the results.

3. Model

3.1. Depth distribution of discontinuities

Zhao et al. (1992) showed that it is effective to conduct inversions by explicitly defining the Conrad, the Moho and the upper boundary of the Pacific slab, in calculating 3-D velocity structure. Also, they emphasized that it is important to adopt accurate depth distribution of these discontinuities.

In this study, we used three discontinuities: the Conrad, the Moho and the upper boundary of the subducting Philippine Sea slab.

We defined the Moho discontinuities by the assumption of isostasy, with the depth data determined by seismic soundings in the Yamato basin (Hirata et al., 1987), the Ogasawara area (Katao et al., 1989) and the Ryukyu area (Iwasaki et al., 1990), and sea floor topography data (Smith and Sandwell, 1994, 1997). We assumed the depth of the Conrad discontinuity to be a half of the Moho depth.

Carr et al. (1973) showed that there were some prominent discontinuities whose offsets were up to 50 km in the deep seismic zones beneath the Ryukyu arc by using the earthquake catalogs of NOAA from 1962 to 1971. This means that the upper boundary of the Philippine Sea slab contains a few prominent discontinuities beneath this region. Moreover, Naganune (1987) showed that the upper boundary of the Philippine Sea slab had the discontinuity whose horizontal offset was 80 km north off Amami-oshima island, by using the earthquake catalogs of ISC from 1971 to 1977 and those of JMA from 1983 to 1985. However, earthquake catalogs used in these studies were less accurate because their hypocenter parameters were determined with a sparser seismic network than the present one (e.g. Seismology and Volcanology Division in Japan Meteorological Agency, 2002). In this study, we compiled depth distribution data of the upper boundary of the Philippine Sea slab using hypocenter parameters as mentioned in Section 2. Then, we could not find any prominent discontinuities. Judging from the grid interval of velocity structure, which is about 30 km, it is reasonable to define explicitly a smooth upper boundary of the Philippine Sea slab.

Fig. 5 shows depth distributions of the three discontinuities defined in this study. In addition, we also conducted inversions without explicitly defining the upper boundary of the Philippine Sea slab to show the effectiveness of the inversion with the slab.

3.2. P-wave velocity structure

The horizontal grid interval was set to 20'. Above the upper boundary of the Philippine Sea slab, vertical grid points were set to the surface, 2, 5, 10 km

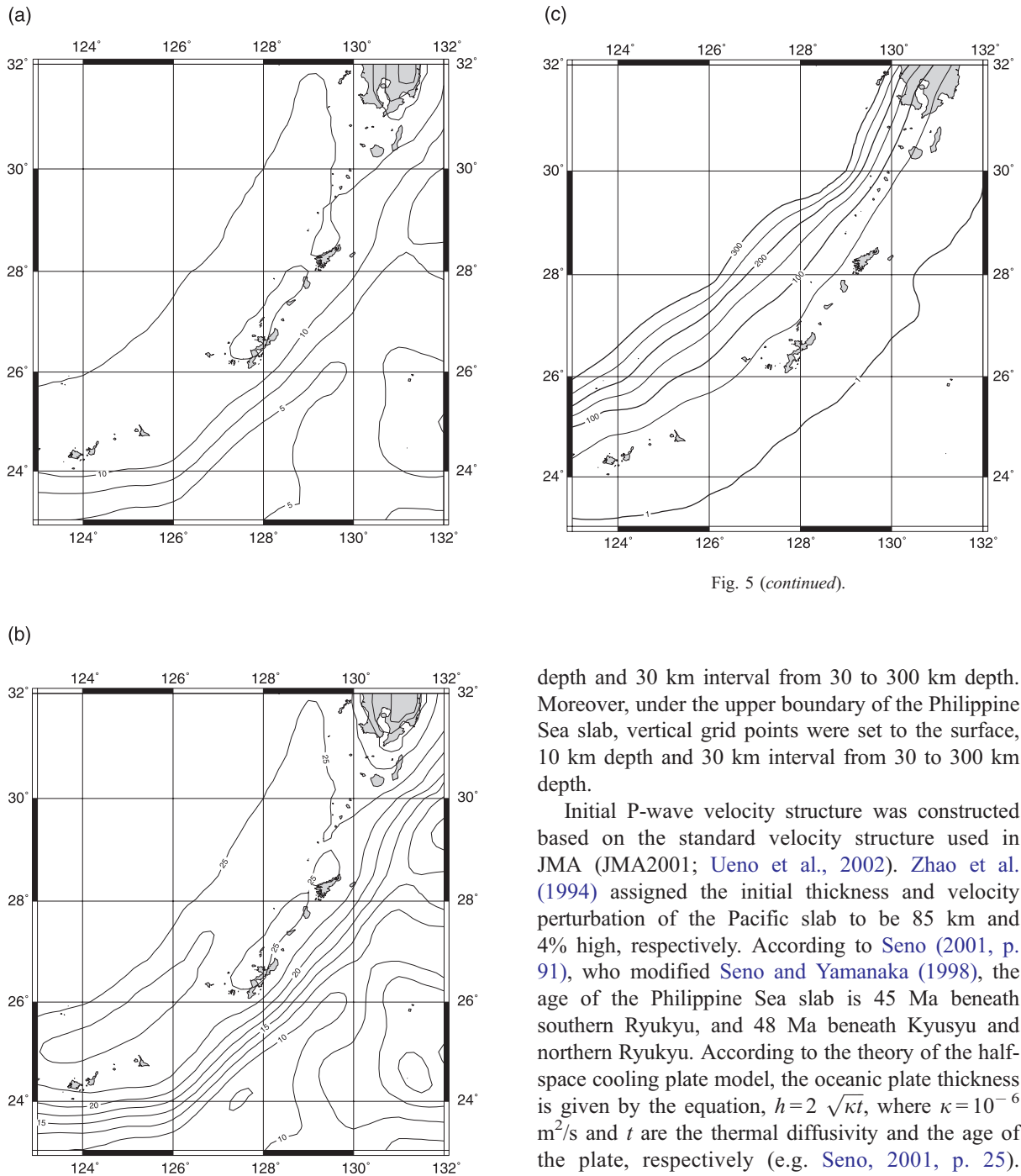


Fig. 5 (continued).

Fig. 5. Depth distribution (unit: km) of (a) the Conrad discontinuity, (b) the Moho discontinuity and (c) the upper boundary of the subducting Philippine Sea slab.

depth and 30 km interval from 30 to 300 km depth. Moreover, under the upper boundary of the Philippine Sea slab, vertical grid points were set to the surface, 10 km depth and 30 km interval from 30 to 300 km depth.

Initial P-wave velocity structure was constructed based on the standard velocity structure used in JMA (JMA2001; Ueno et al., 2002). Zhao et al. (1994) assigned the initial thickness and velocity perturbation of the Pacific slab to be 85 km and 4% high, respectively. According to Seno (2001, p. 91), who modified Seno and Yamanaka (1998), the age of the Philippine Sea slab is 45 Ma beneath southern Ryukyu, and 48 Ma beneath Kyusyu and northern Ryukyu. According to the theory of the half-space cooling plate model, the oceanic plate thickness is given by the equation, $h = 2 \sqrt{\kappa t}$, where $\kappa = 10^{-6} \text{ m}^2/\text{s}$ and t are the thermal diffusivity and the age of the plate, respectively (e.g. Seno, 2001, p. 25). Therefore, we can estimate that the thickness of the Philippine Sea slab is about 75 km in the modeling area. Then, we compared the absolute value of travel time residual (observed travel time – calculated one:

$O - C$) for P-wave, assuming that the thickness of the Philippine Sea slab was 75 km and the velocity perturbation was ranging from 0.0% to 4.0% high, after the relocation of hypocenters, by using the hypocenter parameters and the arrival times as mentioned in Section 2. Fig. 6 shows that the $|O - C|$ became minimum when the velocity perturbation of the Philippine Sea slab was 2.0% high. As a result of this investigation, we assigned the initial thickness and velocity perturbation of the Philippine Sea slab to be 75 km and 2% high, respectively.

To make the initial data set of a simultaneous inversion for P-wave velocity structure and hypocenter parameters, we relocated hypocenters using the 3-D P-wave velocity structure containing the Philippine Sea slab. In this relocation process, we used S-wave arrival times as well as those of P-wave. As for S-wave velocity structure, we assumed that the perturbations of S-wave velocity structure from JMA2001 were similar to those of P-wave. Moreover, the same redetermination of hypocenter parameters was carried out every time after 3-D P-wave velocity structure was updated by the simultaneous inversion. This was because perturbations of hypocenter parameters calculated by the simultaneous inversion sometimes became unstable without S-wave arrival time data.

If station distribution is biased, perturbations of parameters obtained by solving the observation equation may diverge. Also, when the initial hypocenter parameters are nearly equal to true hypocenter

parameters, it is better not to change hypocenter parameter values from the initial so much. Therefore, we redetermined hypocenter parameters under constraint shown in Table 1. Incidentally, when we fixed certain parameters, we just set coefficients of corresponding perturbations in the observation equation to zeros.

We conducted a simultaneous inversion for P-wave velocity structure and hypocenter parameters using the method of Zhao et al. (1994). To make the calculation stable, we excluded the following arrival time data; for data of stations in Minami-daito island, where we observe systematically negative $O - C$ s, arrival times whose $|O - C|$ s were larger than 5 s, and for other data, with $|O - C|$ s larger than 3 s.

Because velocity structure and hypocenter parameters have strong spatio-temporal nonlinear characteristics, we have to repeat the calculation to obtain the solution. Generally speaking, when we repeat the calculation, we changed the damping factor μ in each iteration (e.g. Zhao et al., 1992, 1994). The adequate values of μ depend on the accuracy of arrival times, the resolution of velocity structure and the degree of inhomogeneity. Moreover, we have to obtain a velocity structure which does not depend only on the data set used in the calculation but which also satisfies data sets unused in the calculation. Therefore, we set μ to minimize the average $|O - C|$ for the 2nd best data set in assuming velocity structure which was got every iteration.

We terminated the iteration for solving the observation equation just before the average $|O - C|$ did

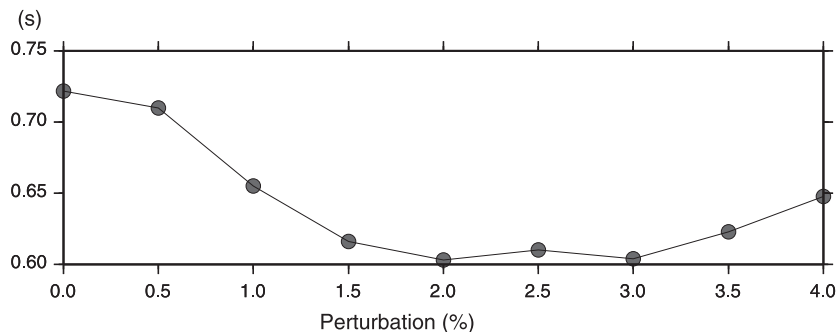


Fig. 6. The average absolute values of the travel time residuals of P-wave for velocity structures whose thicknesses of the Philippine Sea slab were 75 km and velocity perturbations were ranging from 0.0% to 4.0% high.

not become smaller. In the result, we made three iterations for $\mu=10$, $\mu=18$ and $\mu=78$.

Incidentally, because perturbations of hypocenter parameters obtained by solving the observation equation did not take S-wave arrival times into consideration, we did not redetermine hypocenter parameters by these perturbations. Instead, we redetermined hypocenter parameters based on the P-wave velocity structure every time before and after conducting the simultaneous inversion.

3.3. S-wave velocity structure

Onset of S-wave is less clear than that of P-wave, and the number of arrival times of S-wave is less than that of P-wave. So, the determined S-wave velocity structure has a lower resolution and is less accurate than the P-wave velocity structure. Therefore, it is necessary to set the initial velocity structure as accurate as possible to derive the final S-wave velocity structure.

We can assume that the velocity perturbations of S-wave are closely related to those of P-wave. In this study, we applied 3-D P-wave velocity perturbations to get the initial S-wave velocity structure, based on JMA2001.

If we conducted a simultaneous inversion of S-wave velocity structure and hypocenter parameters as for determining P-wave velocity structure, hypocenter parameters might tend to diverge. Therefore, we conducted the inversion of S-wave velocity structure only by fixing hypocenter parameters to those redetermined based on the P-wave velocity structure.

To make the calculation stable, we did not use the following arrival time data; for data of stations in Minami-daito island, arrival times whose $|O - C|$ s were larger than 10 s, and for other data, with $|O - C|$ s larger than 4 s. We made two iterations with the damping factor $\mu=18$ and $\mu=60$.

4. Result and discussion

Figs. 7–10 show the determined 3-D P- and S-wave velocity models (final models) and V_p/V_s values. V_p/V_s values were calculated from the final models. Fig. 11 shows the results of the CRT. Fig. 12 shows the final models, those of the results of the RRT, those of the 3-D P- and S-wave velocity models, which were obtained by analyzing the 2nd best data set by the same method (Model 1). Fig. 13 shows those of the 3-D P- and S-wave velocity models, which were obtained by analyzing without explicitly defining the upper boundary of the Philippine Sea slab (Model 2), in addition to them.

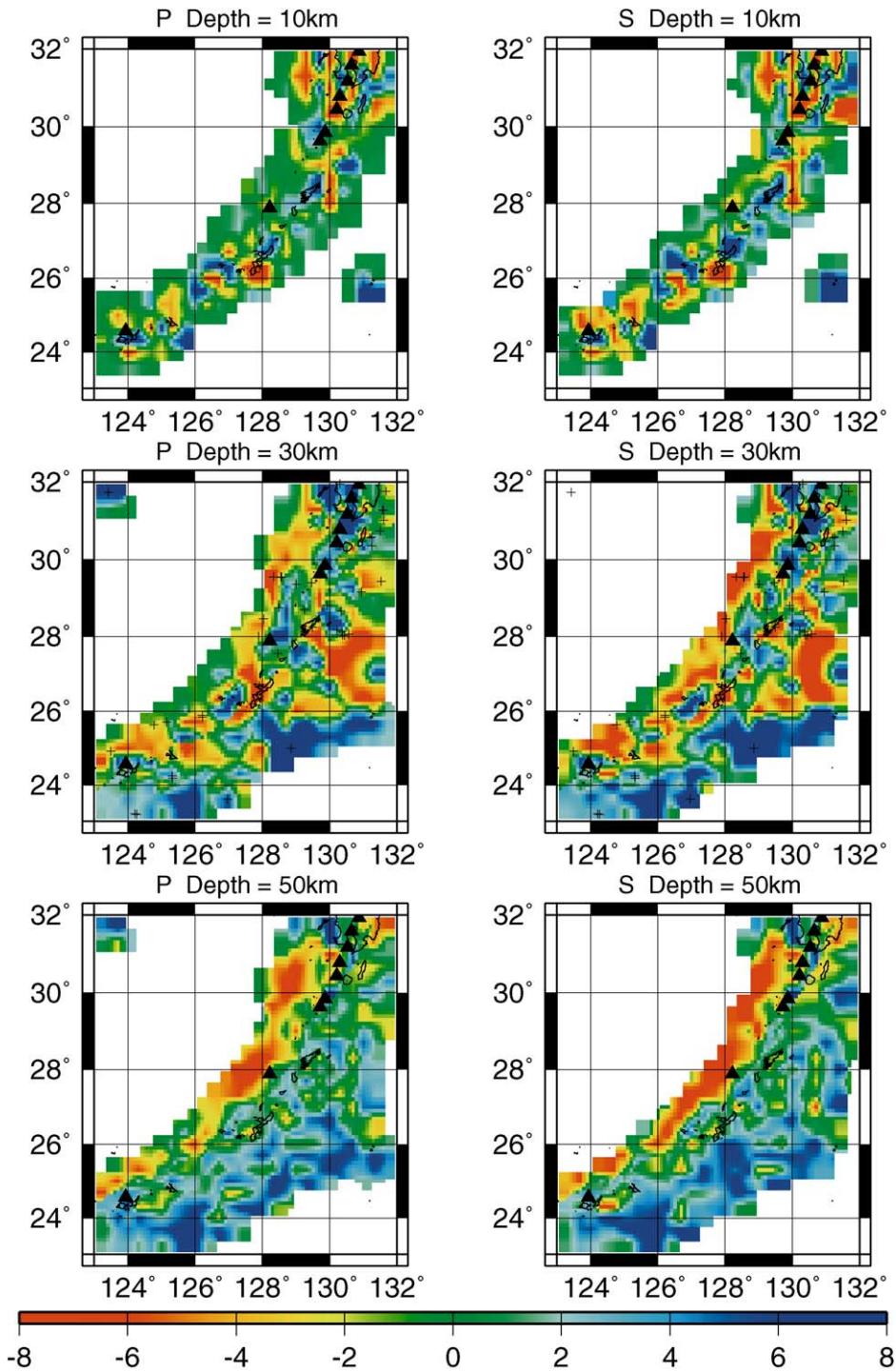
Judging from Fig. 11, the results of the CRT are good around islands for the depth range from 7.5 to 135 km. However, they are not so good in the sea area where stations do not exist. Moreover, on the average, the results of the test are not so good at 195 km depth, but the checkerboard pattern is restored for P-wave in some areas, e.g. southeast off Okinawa island.

Almost all results of the RRT are good at all ranges of depths in the modeling area (Figs. 12 and 13). However, in some regions, the results are not so good. For example, as for the low velocity areas for P- and S-wave north off and west off Minami-daito island at 30 km depth, they are weaker than original ones (Figs. 12b and 13b). The velocity structure assumed in the RRT is very realistic but that assumed in the CRT is rather unrealistic. Therefore, the final models are possibly realistic even in the areas where the results of the CRT are not so good.

The final models are similar to the Model 1, in almost everywhere in the modeling area (Figs. 12 and 13). Therefore, the final models do not depend only on used data set, and the reliability is high.

After we determined the final models, the average $|O - C|$ is reduced from 0.722 to 0.559 s for P-wave and becomes from 1.263 to 0.942 s for S-wave. To see the effect of the high velocity Philippine Sea slab, we

Fig. 7. The horizontal cross sections of determined 3-D P- (left figures) and S-wave (right figures) velocity models (final models) at 10 km (upper figures), 30 km (middle figures) and 50 km depth (lower figures). The velocity perturbations (%) from an average velocity at each depth are shown. In each figure, active volcanoes, which were selected by JMA (e.g. Japan Meteorological Agency, 2000), are plotted simultaneously (solid triangles). Moreover, in middle figures, epicenters of earthquakes (from March 1987 to March 2002, $M \geq 5.5$, depth ≤ 60 km), which were determined by JMA, are plotted simultaneously (plus symbols).



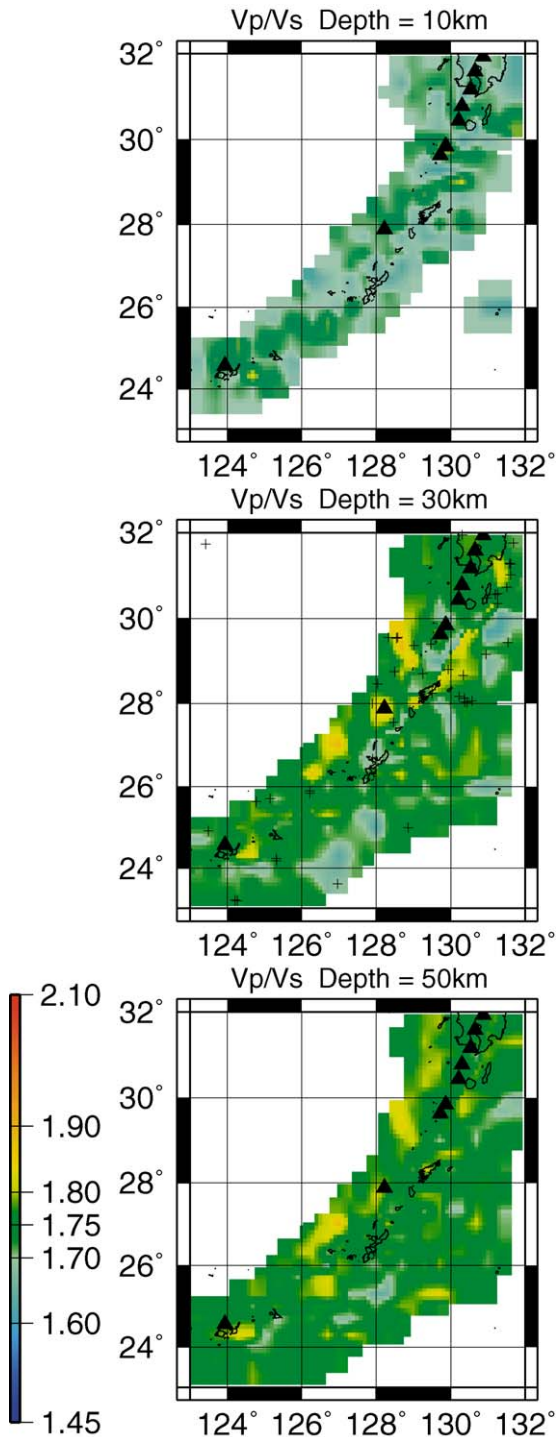
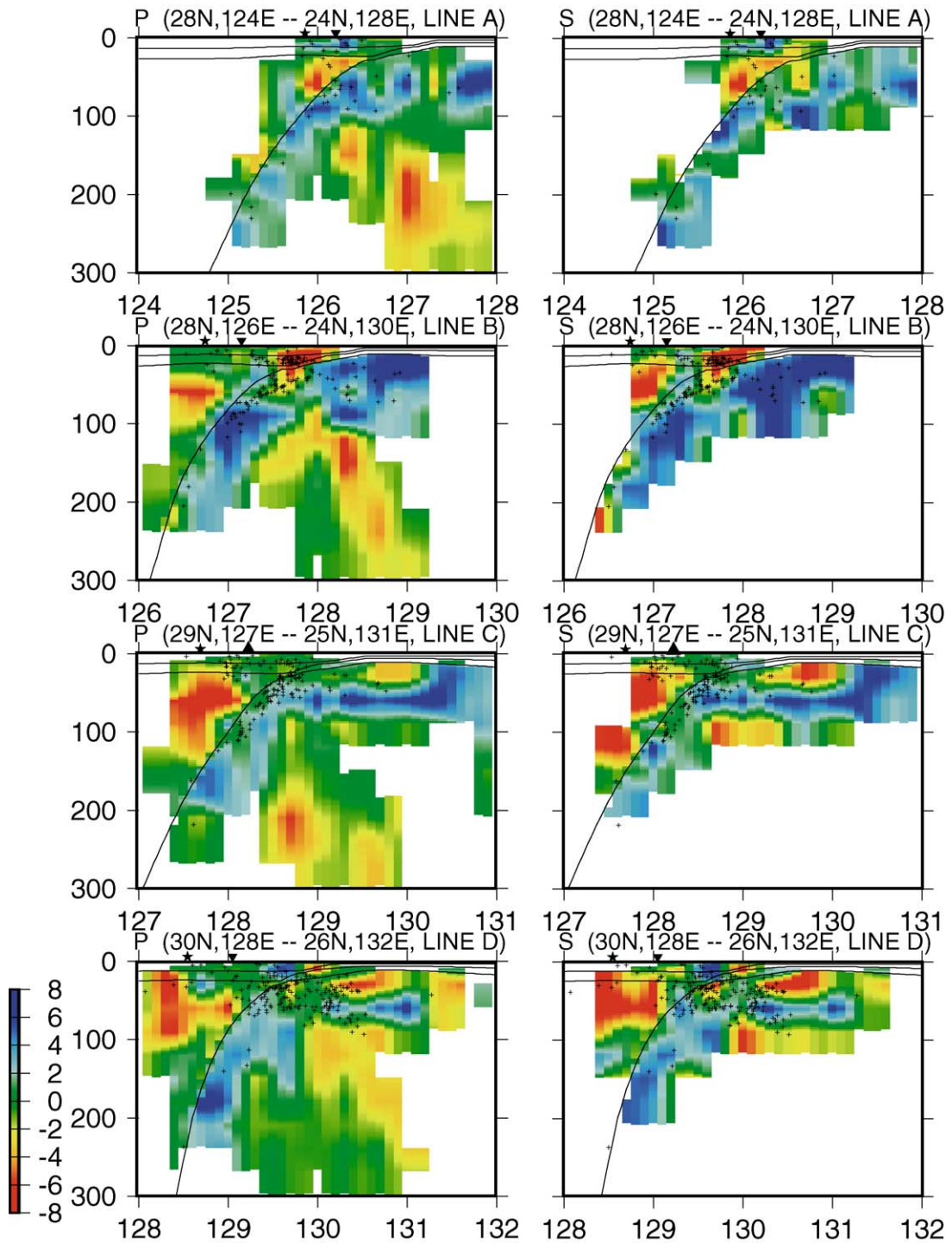


Fig. 8. The horizontal cross sections of V_p/V_s values at 10 km (the upper figure), 30 km (the middle figure) and 50 km depth (the lower figure).

conducted the following calculations. By assuming the initial P-wave velocity structure, the average $|O - C|$ becomes 0.603 s for P-wave and 1.043 s for S-wave. This means that we can reduce the $|O - C|$ s 73% for P-wave and 69% for S-wave, by explicitly defining the high velocity Philippine Sea slab. Moreover, by using the Model 2, the average $|O - C|$ was 0.634 s for P-wave and 1.158 s for S-wave. Furthermore, by comparing the Model 2 with the final model, the upper boundary of the Philippine Sea slab is less clear, and the amplitude of some high velocity areas under the boundary is less prominent (Fig. 13). Judging from these, it seems very effective to introduce explicitly the upper boundary of the Philippine Sea slab into the model.

At stations in Minami-daito island (stars in Fig. 4), we observe a systematically negative $O - C$, when we calculate hypocenter parameters with JMA2001. Fig. 14a shows the distribution of $O - C$ s for the data set used in this study. These figures show that the distribution of $O - C$ s for P-wave has a peak around -4 s except for the one around 0 s, which is usually seen, and that the distribution of $O - C$ s for S-wave does not have a notable peak and most of the data are in the range between $+1$ and -6 s. Fig. 14b shows the distribution of $O - C$ s for the stations in Minami-daito island, calculated with the initial P-wave velocity structure. Similarly, Fig. 14c is the distribution of $O - C$ s for the stations in Minami-daito island, calculated with the final models and the hypocenter parameters obtained in this study. These figures show that the systematically negative $O - C$ shown in Fig. 14a almost disappears by the analysis. Furthermore, these figures show that the reason of the systematically negative $O - C$ is not only the existence of the high

Fig. 9. The vertical cross sections of the determined 3-D P- (left figures) and S-wave (right figures) velocity models (final models) along the lines A, B, C and D in Fig. 4. In each figure, solid triangles on the top represent active volcanoes near the sections. If there is no active volcano near the sections, solid inverse triangles on the top represent the positions of the volcanic front. Solid stars on the top represent the positions of the Okinawa trough at the sections. Earthquakes that occurred near the sections (initial hypocentral locations of earthquakes used in this study) are plotted simultaneously (plus symbols). Furthermore, the Conrad discontinuity, the Moho discontinuity and the upper boundary of the subducting Philippine Sea slab, which were explicitly defined, are drawn simultaneously.



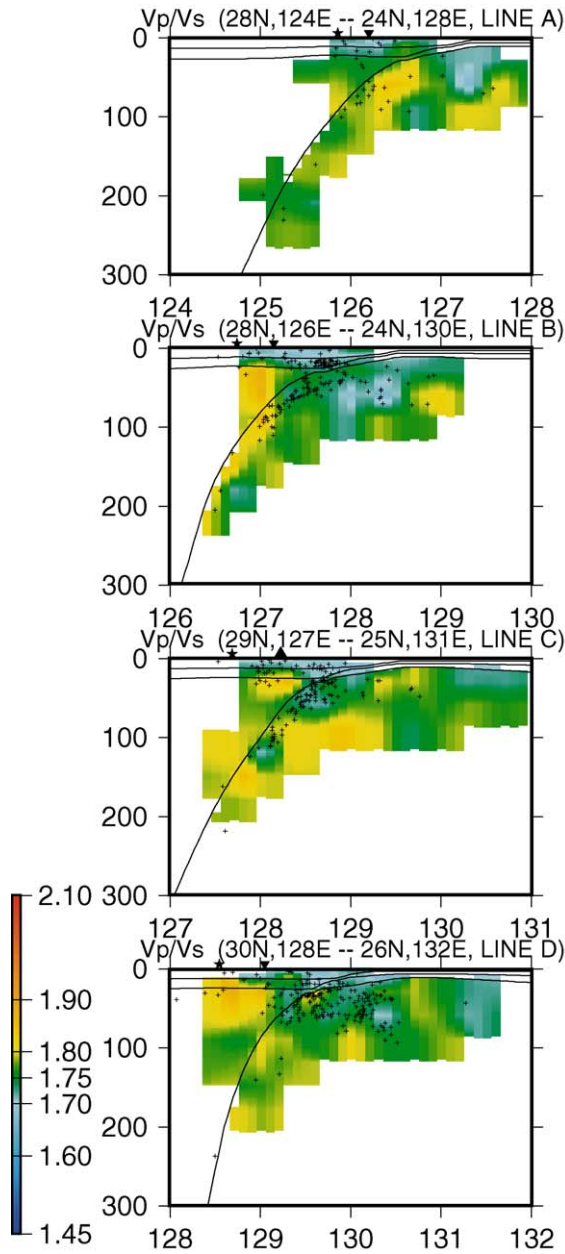


Fig. 10. The vertical cross sections of Vp/Vs values along the lines A, B, C and D in Fig. 4.

velocity Philippine Sea slab, but also the heterogeneity in the 3-D structure.

P- and S-wave low velocity zones exist just beneath active volcanoes at about 10 km depth (upper

figures in Fig. 7). Also, relatively high Vp/Vs zones exist there (the upper figure in Fig. 8). These zones most likely reflect the influence of magmas beneath the active volcanoes. These results are similar to those that have already been shown by many researchers for other areas (e.g. Zhao et al., 1994, 1995). Around these areas, the results of the RRT are generally good (Fig. 12a). The final models are similar to the Model 1 (Fig. 12a). Furthermore, the result of the CRT is almost good in most cases (Fig. 11a). Therefore, the reliability seems to be high.

Prominent P- and S-wave low velocity zones exist along the Okinawa trough at about 50 km depth (lower figures in Fig. 7). In these areas, Vp/Vs values are high (the lower figure in Fig. 8). The Okinawa trough is a backarc basin whose rifting is still in progress (e.g. Park et al., 1998). The gravity anomaly map of Japan and adjoining areas (Geological Survey of Japan, 1992) shows that the trough has slightly positive Bouguer anomalies. Moreover, the heat flow map of east and southeast Asia (Geological Survey of Japan, 1997) shows that the trough exhibits a high heat flow. We consider that the low-velocity and high Vp/Vs anomalies represent some mantle materials flow upward from the depth greater than 50 km along the trough. Around these areas, the result of the RRT is good (Fig. 12c). Moreover, the final models are similar to the Model 1 (Fig. 12c). Also, the result of the CRT is excellent (Fig. 11a). Therefore, these features are reliable.

In the vertical cross sections of the final P-wave model, prominent low velocity anomalies exist beneath the high velocity Philippine Sea slab (Fig. 9). These anomalies were obtained by the arrival times for teleseismic events. These anomalies are also shown in the results of the RRT, in the Model 1 and in the Model 2 (Fig. 13). The results of the CRT are not so good, but the checkerboard pattern is reproduced in some areas, e.g. southeast off Okinawa island (Fig. 11b). Therefore, we tried to confirm the validity of those low velocity anomalies, by the same procedure of the RRT with initial P-wave velocity structure containing the high velocity Philippine Sea slab. In Fig. 15, we show the vertical cross sections of the test results for P- and S-wave velocity structures, along the lines A and D in Fig. 4. In the figure, slightly low velocity anomalies exist beneath the high velocity Philippine Sea slab, but the anomalies shown in Figs. 9 and 13 are more

distinct than those in Fig. 15. Judging from these test results, these low velocity anomalies in Figs. 9 and 13 are probably true. Zhao et al. (1994) showed that low velocity anomalies exist in the mantle beneath the Pacific slab, and they pointed out that they are possibly associated with small-scale mantle convections. The prominent low velocity anomalies beneath the Philippine Sea slab obtained in this study may reflect the same process.

Around the Ryukyu arc, a new data transmission system was started in March 1987, and seismological observation data in this area have been improved in quality and quantity (Seismology and Volcanology Division in Japan Meteorological Agency, 2002). In the cross sections at 30 km depth in Figs. 7 and 8, the hypocenters of earthquakes, which occurred from March 1987 to March 2002, with $M \geq 5.5$ and depth ≤ 60 km, and which were determined by JMA, are plotted simultaneously. These figures show that these earthquakes generally occurred at the edge portions of P- and S-wave low velocity zones and of high V_p/V_s value zones at about 30 km depth. Zhao et al. (2000) insisted that large crustal earthquakes occurred in and around the P-wave low velocity zones. Then, they considered that P-wave low velocity zones might represent weak sections of the seismogenic crust, caused by active volcanoes, magma chambers and the dehydration of the subducting slabs. Earthquakes shown in Figs. 7 and 8 consist of not only crustal earthquakes but also interplate earthquakes, but we cannot distinguish them for the reason of inaccuracy of the hypocenter determination especially in depth, which are partly caused by the sparse seismic network in this area. The clarification of this problem will be a future topic.

5. Conclusions

1. We obtained the 3-D P- and S-wave velocity structures beneath the Ryukyu arc, which are more accurate than the previous studies.
2. It is effective to conduct inversions by explicitly introducing the subducting Philippine Sea slab into the model in calculating 3-D velocity structure beneath the Ryukyu arc.
3. The reason of systematically negative $O - C_s$ in the stations in Minami-daito island in assuming a spherically layered velocity structure, is not only the existence of the high velocity Philippine Sea slab, but also the heterogeneity in the 3-D structure.
4. P- and S-wave low velocity zones and high V_p/V_s zones exist just beneath active volcanoes at about 10 km depth. These zones reflect the influence of magmas beneath the active volcanoes.
5. Prominent P- and S-wave low velocity zones exist along the Okinawa trough at about 50 km depth. In these zones, V_p/V_s values are high. The low-velocity and high V_p/V_s anomalies will represent some mantle materials flow upward from the depth greater than 50 km along the trough.
6. Low velocity anomalies exist beneath the Philippine Sea slab, which are possibly associated with small-scale mantle convections.

Acknowledgements

We would like to express our gratitude to Dr. A. Yoshida, Mr. H. Takayama, and ex-director Dr. K. Horai in Meteorological Research Institute for valuable discussions. We thank members of related organizations (National Research Institute for Earth Science and Disaster Prevention, Hokkaido University, Hirosaki University, Tohoku University, the University of Tokyo, Nagoya University, Kyoto University, Kochi University, Kyusyu University, Kagoshima University, National Institute of Advanced Industrial Science and Technology, Tokyo Prefecture, Hot Springs Research Institute of Kanagawa Prefecture, Shizuoka Prefecture, Yokohama City, Japan Marine Science and Technology Center and JMA) of which high sensitivity seismogram data are transmitted to a cooperative system of JMA and Ministry of Education, Culture, Sports, Science and Technology, who operate the routine observation network, for supplying valuable data. Our gratitude is also extended to members of Kyoto University, Seismology and Volcanology Division in JMA, Fukuoka District Meteorological Observatory and Okinawa Meteorological Observatory, who operate the temporary pop-up type ocean bottom

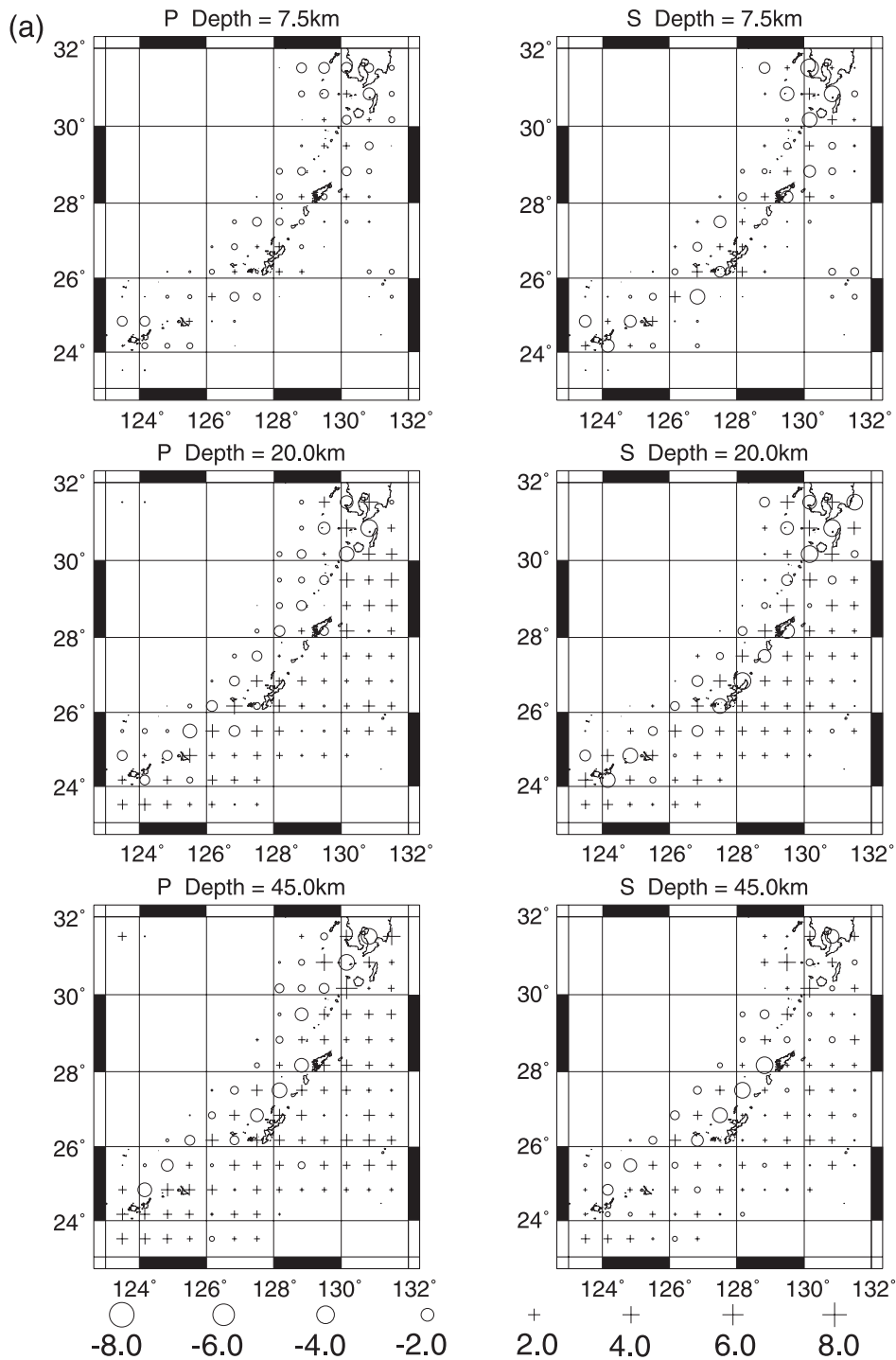


Fig. 11. (a) The horizontal cross sections of the results of the checkerboard resolution test at 7.5 km (upper figures), 20 km (middle figures) and 45 km depth (lower figures) for 3-D P- (left figures) and S-wave (right figures) velocity structures in assuming the checkerboard intervals are about 30 km. (b) The horizontal cross sections at 75 km (upper figures), 135 km (middle figures) and 195 km depth (lower figures).

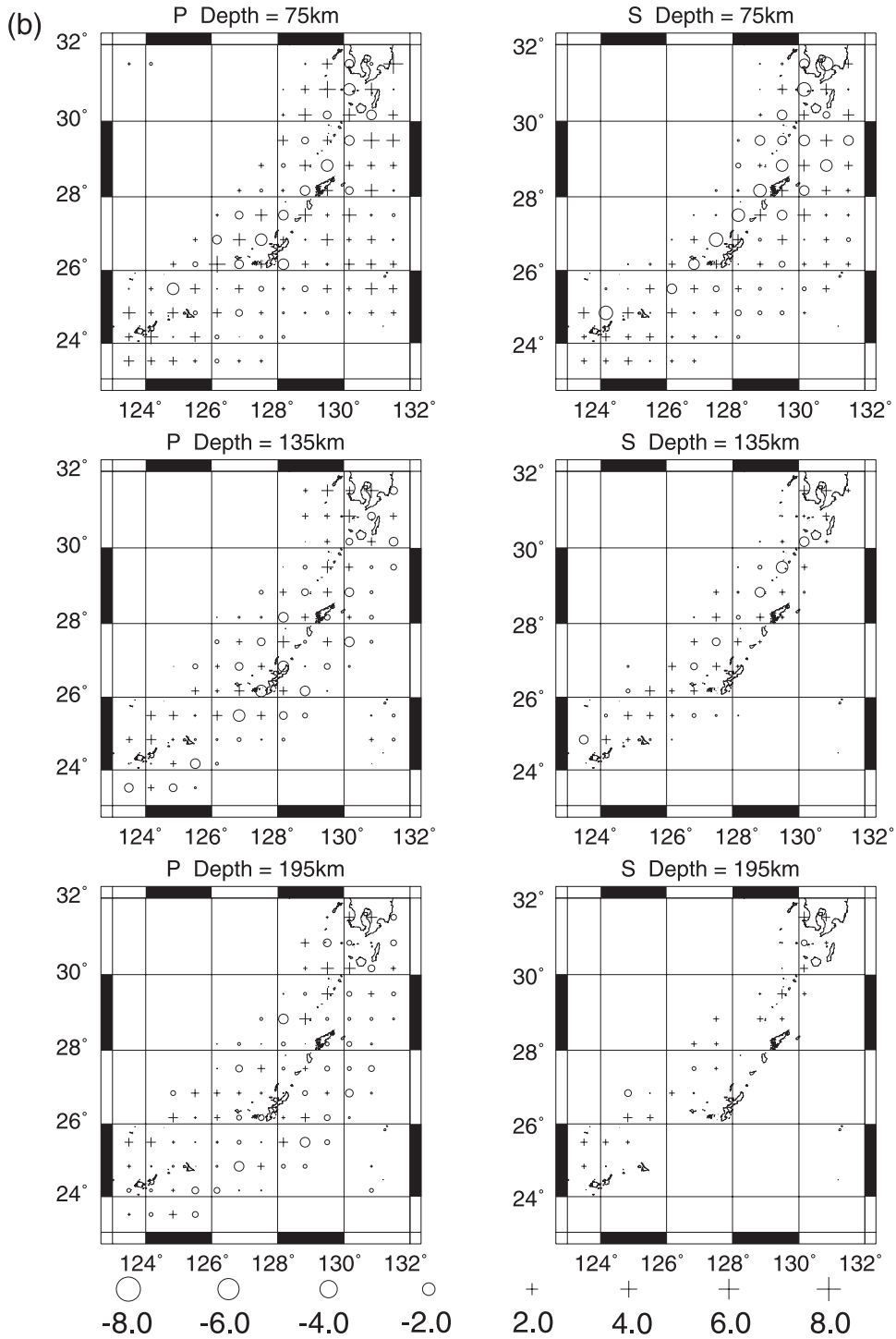


Fig. 11 (continued).

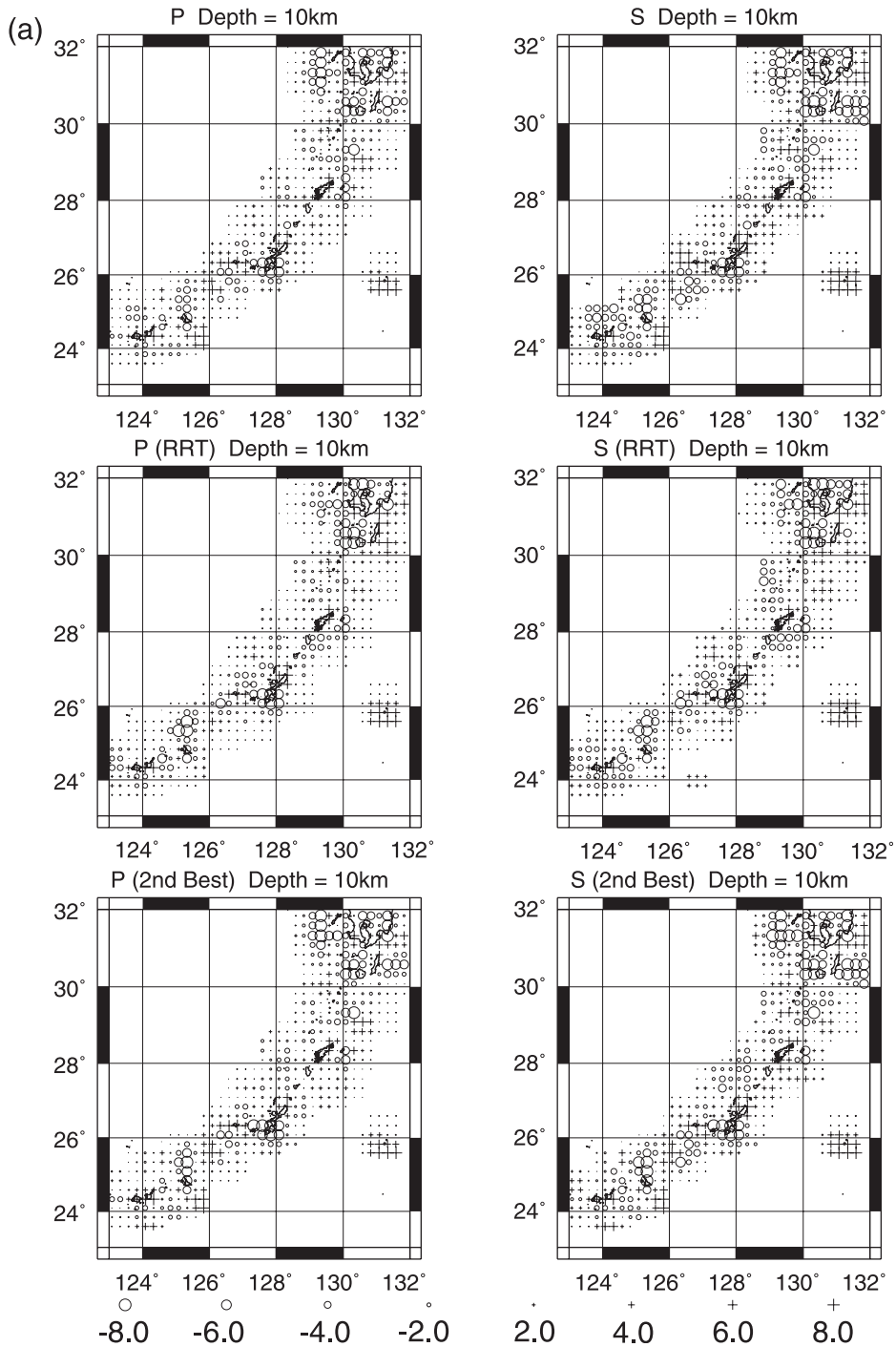


Fig. 12. (a) The horizontal cross sections of the determined 3-D P- (upper left) and S-wave (upper right) velocity models (final models; the same as upper figures in Fig. 7), those of the results of the restoring resolution test (RRT; middle figures) and those of the 3-D P- (lower left) and S-wave (lower right) velocities, which were obtained by analyzing the 2nd best data set (see the text in Section 2) by the same method (Model 1), at 10 km depth. (b) The horizontal cross sections at 30 km depth. (c) The horizontal cross sections at 50 km depth.

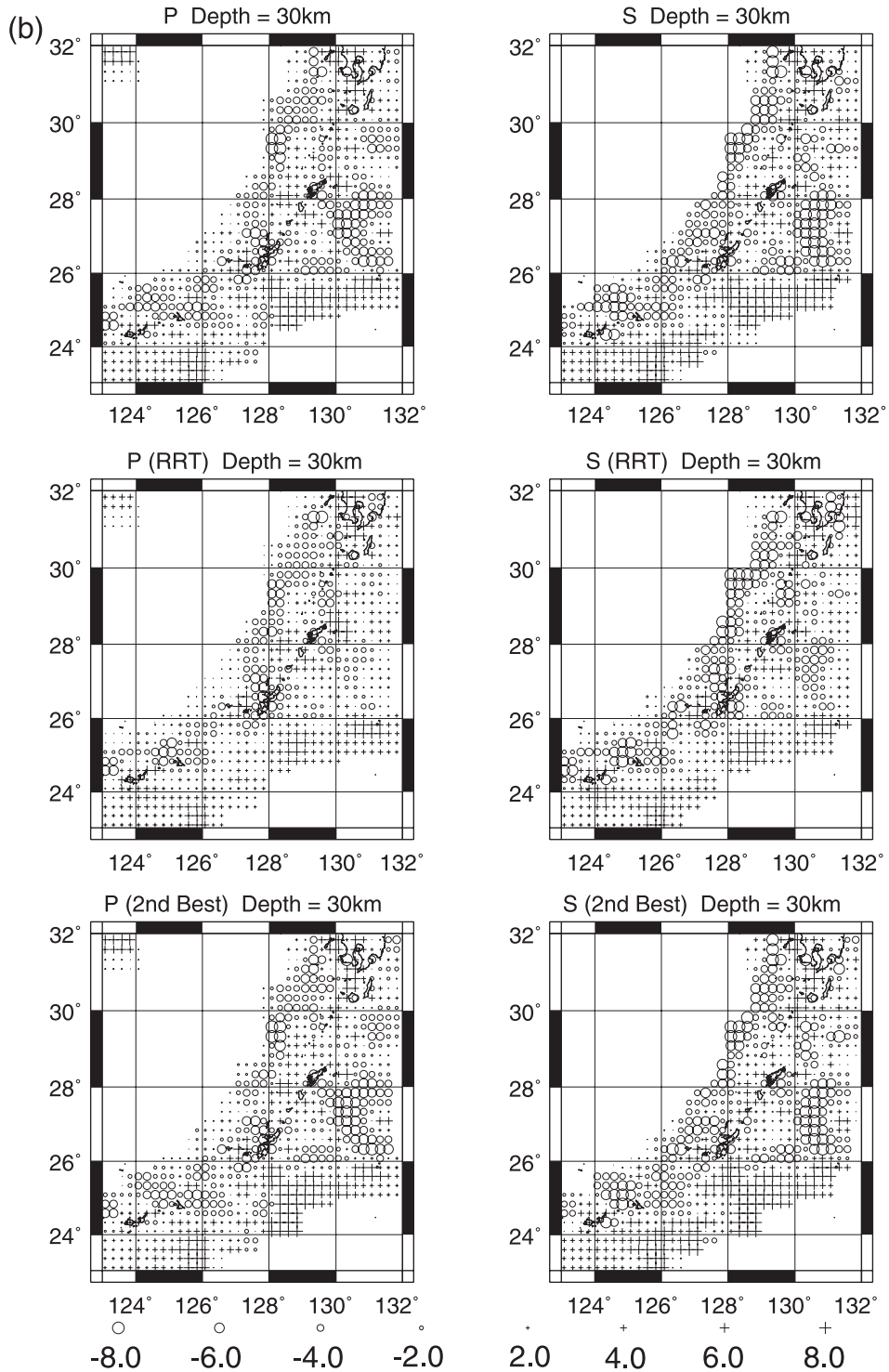


Fig. 12 (continued).

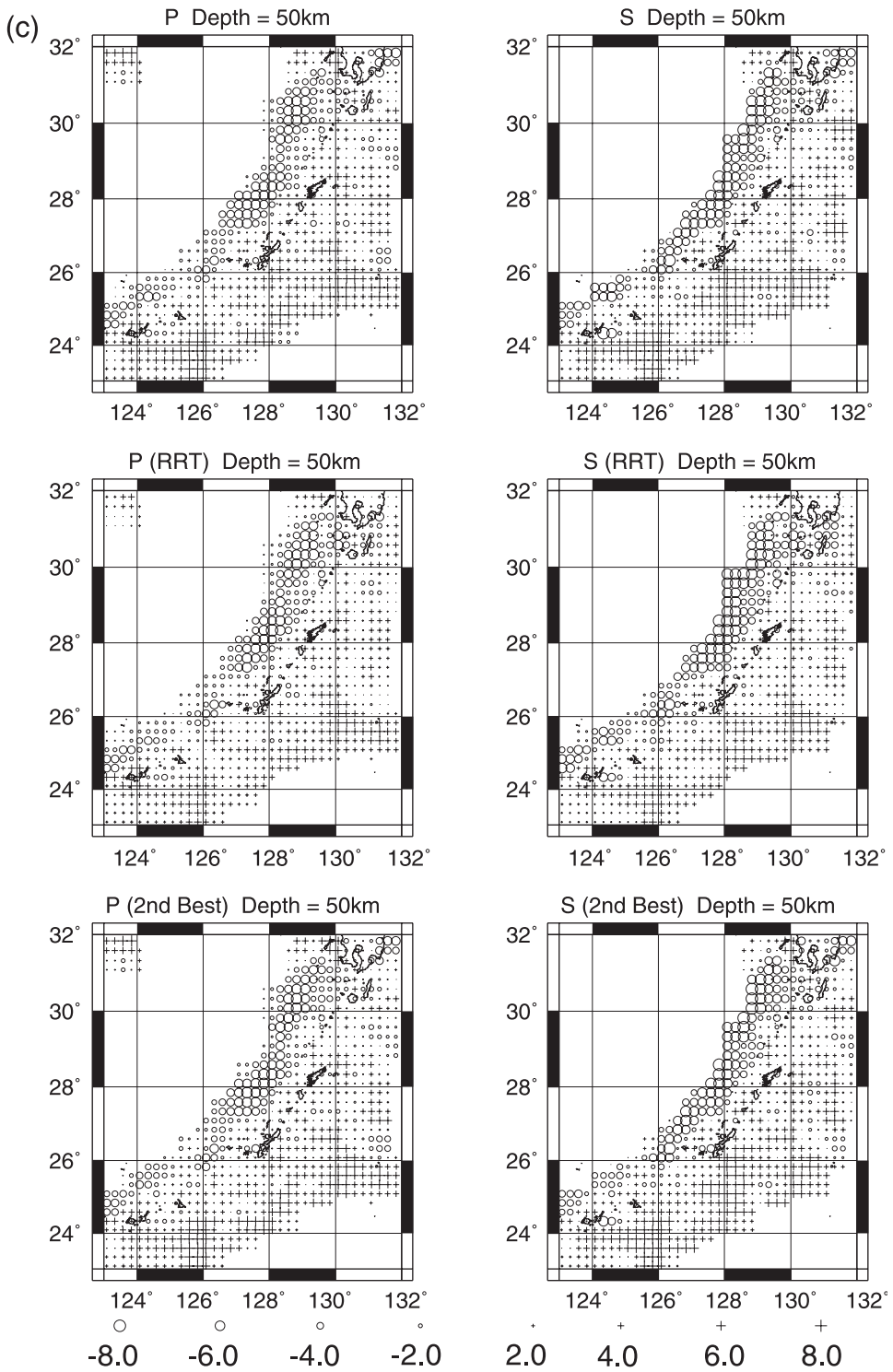


Fig. 12 (continued).

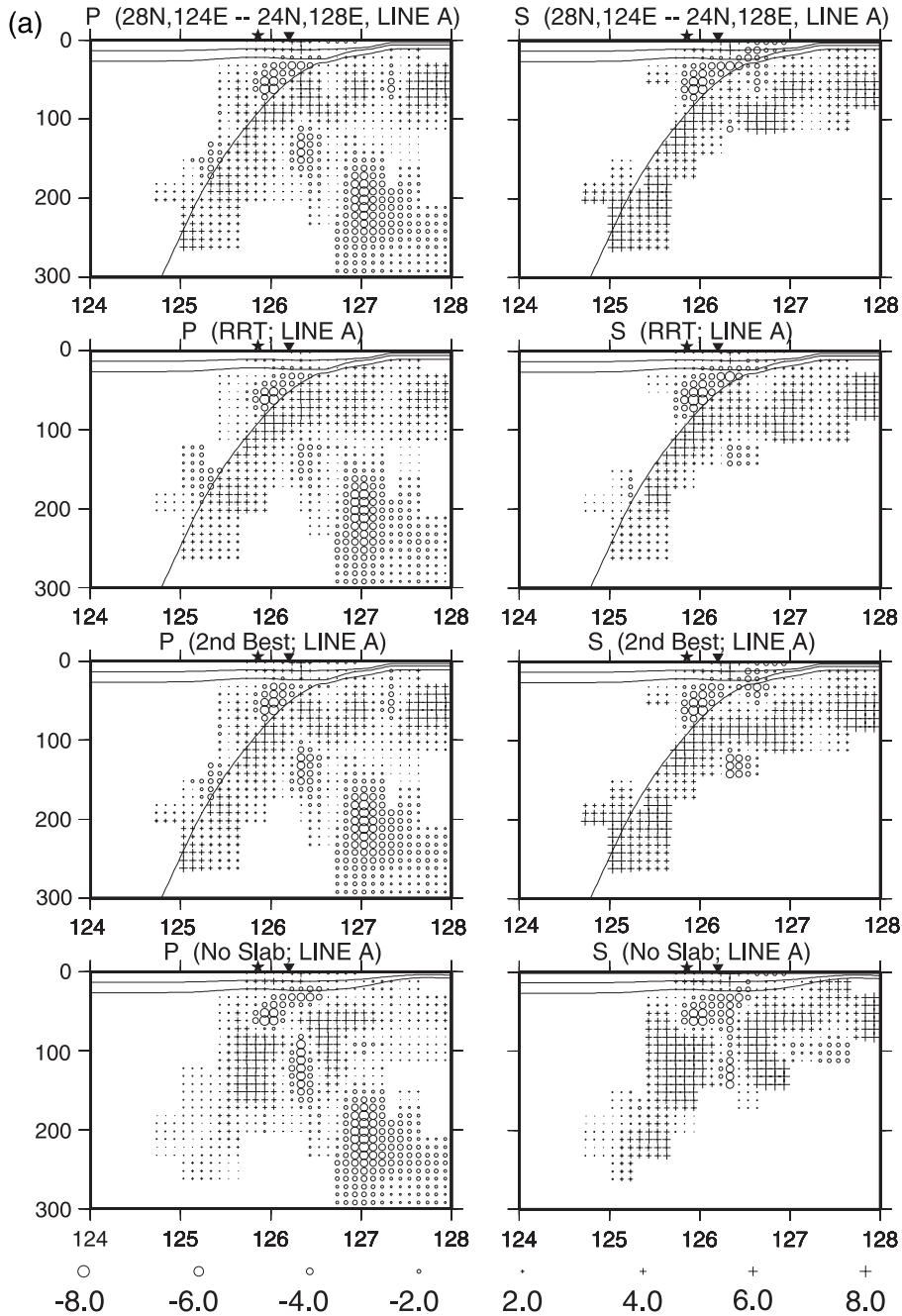


Fig. 13. (a) The vertical cross sections of the determined 3-D P- (left) and S-wave (right) velocity models (final models; the same as Fig. 9), those of the results of the restoring resolution test (RRT), those of the 3-D P- and S-wave velocities, which were obtained by analyzing the 2nd best data set (see the text in Section 2) by the same method (Model 1), and those of the 3-D P- and S-wave velocities, which were obtained by analyzing without explicitly defining the upper boundary of the Philippine Sea slab (No Slab: Model 2), along the line A in Fig. 4. (b) The vertical cross sections along the line D in Fig. 4.

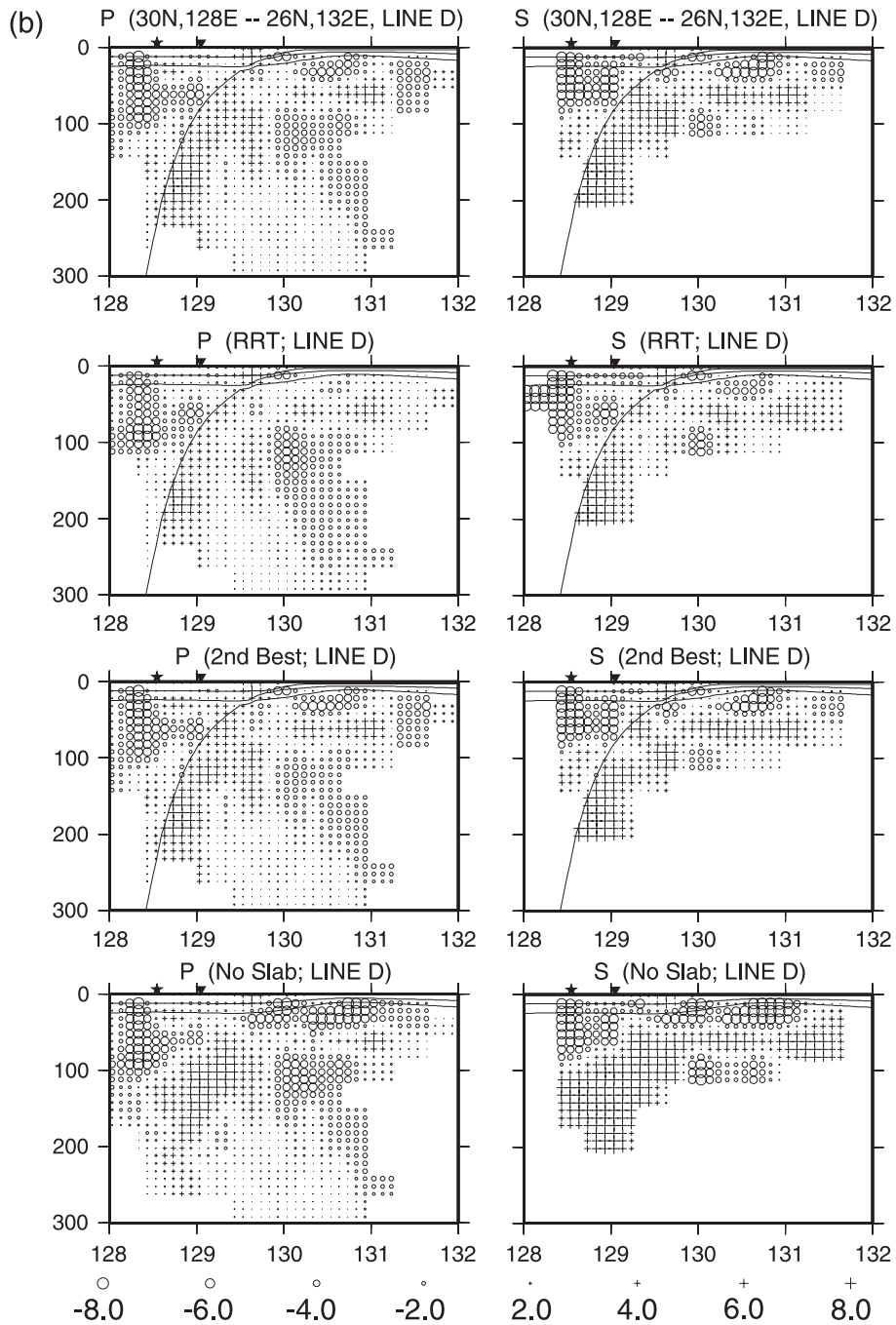


Fig. 13 (continued).

seismometer networks near Tanegashima island, southeast off Tokara islands and southwest off Kumejima island, for providing useful data. We

appreciate the valuable comments and the reviews of the editor and referees, who helped to improve the manuscript. We used Generic Mapping Tools

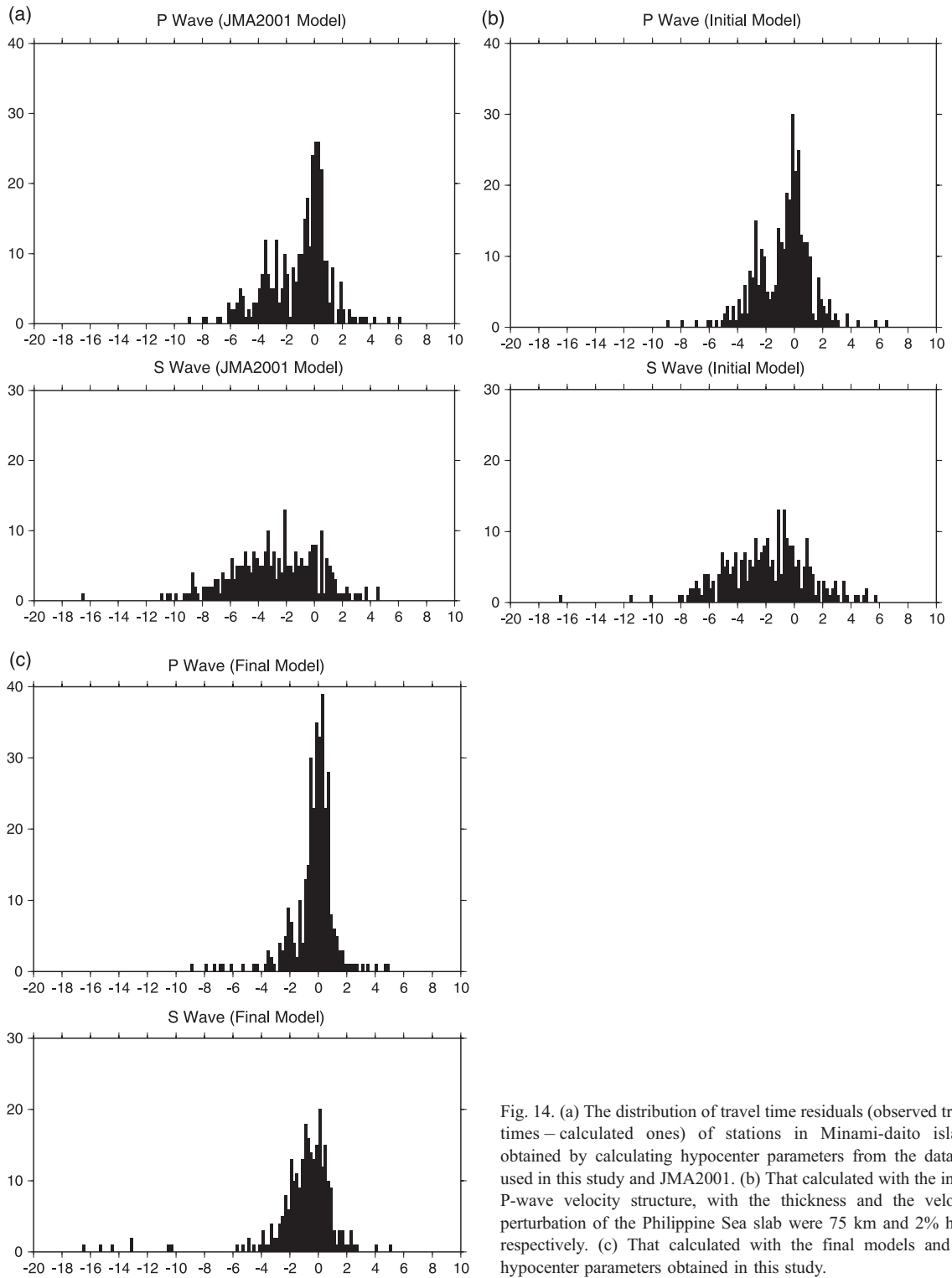


Fig. 14. (a) The distribution of travel time residuals (observed travel times – calculated ones) of stations in Minami-daito island, obtained by calculating hypocenter parameters from the data set used in this study and JMA2001. (b) That calculated with the initial P-wave velocity structure, with the thickness and the velocity perturbation of the Philippine Sea slab were 75 km and 2% high, respectively. (c) That calculated with the final models and the hypocenter parameters obtained in this study.

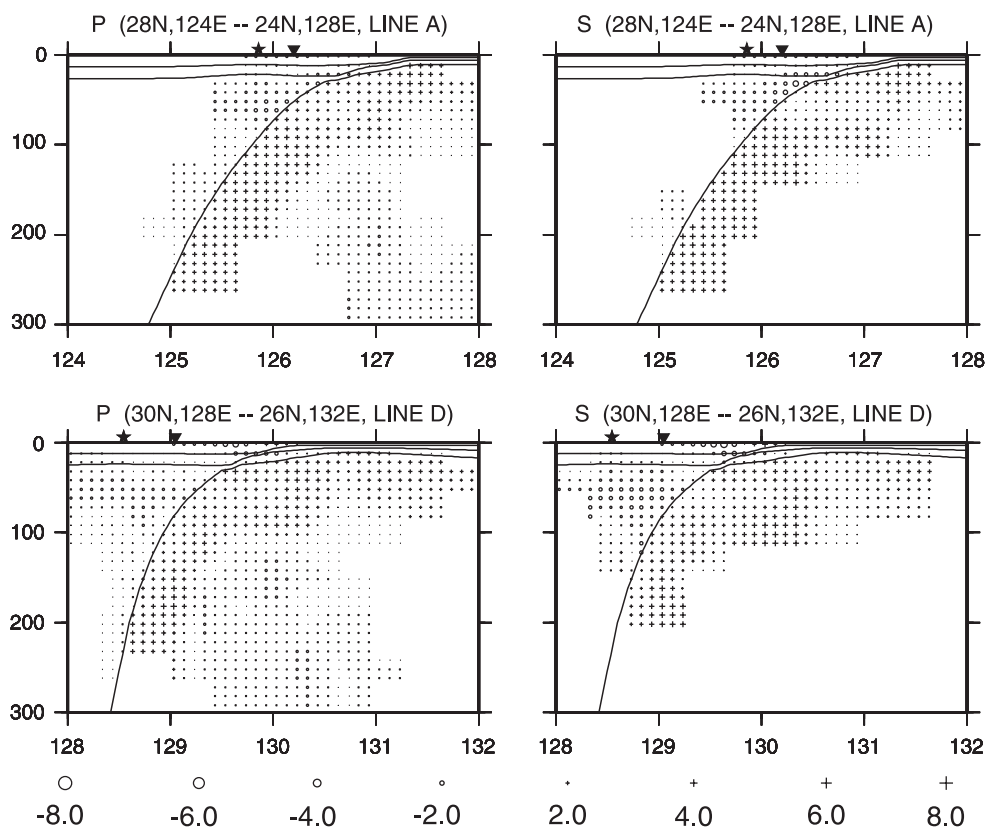


Fig. 15. The results of the restoring resolution test for initial P-wave velocity structure, with the thickness and the velocity perturbation of the Philippine Sea slab were 75 km and 2% high, respectively. The vertical cross sections of the test results for P- (left) and S-wave (right) velocity structures are shown, along the lines A and D in Fig. 4.

(Wessel and Smith, 1995) to make some figures in this paper.

References

- Carr, M.J., Stoiber, R.E., Drake, C.L., 1973. Discontinuities in the deep seismic zones under the Japanese arcs. *Geol. Soc. Am. Bull.* 84, 2917–2930.
- Geological Survey of Japan, 1992. Gravity Anomaly Map of Japan and Adjoining Areas. Geological Survey of Japan, Ibaraki.
- Geological Survey of Japan, 1997. Heat Flow Map of East and Southeast Asia. Geological Survey of Japan, Ibaraki.
- Hirata, N., Kinoshita, H., Suyehiro, K., Suyemasu, M., Matsuda, N., Ouchi, T., Katao, H., Koresawa, S., Nagumo, S., 1987. Report on DELP 1985 cruises in the Japan Sea Part II: seismic refraction experiment conducted in the Yamato basin, southeast Japan Sea. *Bull. Earthq. Res. Inst.* 62, 347–365.
- Inoue, H., Fukao, Y., Tanabe, K., Ogata, Y., 1990. Whole mantle P-wave travel time tomography. *Phys. Earth Planet. Inter.* 59, 294–328.
- Iwasaki, T., Hirata, N., Kanazawa, T., Melles, J., Suyehiro, K., Urabe, T., Möller, L., Makris, J., Shimamura, H., 1990. Crustal and upper mantle structure in the Ryukyu Island arc deduced from deep seismic sounding. *Geophys. J. Int.* 102, 631–651.
- Japan Meteorological Agency, 2000. The Seismological and Volcanological Bulletin of Japan for January 2000. Japan Meteorological Agency, Tokyo, pp. 53–55.
- Kamiya, S., 1991. Three-dimensional P-wave velocity structure beneath the Japanese Islands estimated from the seismological bulletin of the Japan Meteorological Agency. *Zisin (J. Seismol. Soc. Jpn.)* 44, 185–201 (in Japanese, with English abstract).
- Kamiya, S., Miyatake, T., Hirahara, K., 1989. Three-dimensional P-wave velocity structure beneath the Japanese Islands. *Bull. Earthq. Res. Inst.* 64, 457–485.
- Katao, H., Hino, R., Nagumo, S., Koresawa, S., Nishizawa, A., Suyehiro, K., Kubo, A., Ouchi, T., Ishibashi, M., Ono, Y., Baba, H., Kinoshita, H., 1989. Report on DELP 1987 Cruises in the

- Ogasawara area Part IV: explosion seismic refraction studies. *Bull. Earthq. Res. Inst.* 64, 163–177.
- Nagamune, T., 1987. Intermediate-depth earthquakes and tectonics of the Kyushu–Ryukyu region. *Zisin (J. Seismol. Soc. Jpn.)* 40, 417–423 (in Japanese, with English abstract).
- Nakamura, M., Yoshida, Y., Kuroki, H., Yoshikawa, K., Zhao, D., Takayama, H., Yamazaki, T., Fujiwara, K., Hamada, N., Kasahara, J., Kanazawa, T., Kodaira, S., Sato, T., Shiobara, H., Hino, R., 2000. Three-dimensional P and S wave velocity structure beneath Japan. Programme and Abstracts the Seismological Society of Japan 2000, Fall Meeting, P50 (in Japanese).
- Paige, C.C., Saunders, M.A., 1982. LSQR: an algorithm for sparse linear equations and sparse least squares. *ACM Trans. Math. Softw.* 8, 43–71.
- Park, J., Tokuyama, H., Shinohara, M., Suyehiro, K., Taira, A., 1998. Seismic record of tectonic evolution and backarc rifting in the southern Ryukyu Island arc system. *Tectonophysics* 294, 21–42.
- Seismology and Volcanology Division in Japan Meteorological Agency, 2002. The history of earthquake observation in Japan Meteorological Agency. *Q. J. Seismol. Suppl.* 65, 1–401 (in Japanese).
- Seno, T., 2001. More Fundamentals of Plate Tectonics. Asakura, Tokyo. 25 and 91 pp. (in Japanese).
- Seno, T., Yamanaka, Y., 1998. Arc stresses determined by slabs: implications for mechanisms of back-arc spreading. *Geophys. Res. Lett.* 25, 3227–3230.
- Smith, W.H.F., Sandwell, D.T., 1994. Bathymetric prediction from dense altimetry and sparse shipboard bathymetry. *J. Geophys. Res.* 99, 21803–21824.
- Smith, W.H.F., Sandwell, D.T., 1997. Global sea floor topography from satellite altimetry and ship depth soundings. *Science* 277, 1956–1962.
- Ueno, H., Hatakeyama, S., Aketagawa, T., Funasaki, J., Hamada, N., 2002. Improvement of hypocenter determination procedures in the Japan Meteorological Agency. *Q. J. Seismol.* 65, 123–134 (in Japanese, with English abstract).
- Wessel, P., Smith, W.H.F., 1995. New version of the generic mapping tools released. *EOS Trans. Am. Geophys. Union* 76, 329.
- Zhao, D., Hasegawa, A., Horiuchi, S., 1992. Tomographic imaging of P and S wave velocity structure beneath northeastern Japan. *J. Geophys. Res.* 97, 19909–19928.
- Zhao, D., Hasegawa, A., Kanamori, H., 1994. Deep structure of Japan subduction zone as derived from local, regional, and teleseismic events. *J. Geophys. Res.* 99, 22313–22329.
- Zhao, D., Christensen, D., Pulpan, H., 1995. Tomographic imaging of the Alaska subduction zone. *J. Geophys. Res.* 100, 6487–6504.
- Zhao, D., Ochi, F., Hasegawa, A., Yamamoto, A., 2000. Evidence for the location and cause of large crustal earthquakes in Japan. *J. Geophys. Res.* 105, 13579–13594.